Effects of ultraviolet soaking on surface electronic structures of solution processed ZnO nanoparticle films in polymer solar cells

Qinye Bao, Xianjie Liu, Yuxin Xia, Feng Gao, Louis-Dominique Kauffmann, Olivier Margeat, Jorg Ackermann and Mats Fahlman

Original Publication:

Qinye Bao, Xianjie Liu, Yuxin Xia, Feng Gao, Louis-Dominique Kauffmann, Olivier Margeat, Jorg Ackermann and Mats Fahlman, Effects of ultraviolet soaking on surface electronic structures of solution processed ZnO nanoparticle films in polymer solar cells, 2014, Journal of Materials Chemistry A, (2), 41, 17676-17682.
http://dx.doi.org/10.1039/c4ta02695k

Effects of ultraviolet soaking on surface electronic structure of solution processed ZnO nanoparticle film in polymer solar cell

Qinye Bao[1], Xianjie Liu[1], Yuxin Xia [1], Feng Gao[1], Louis-Dominique Kauffmann[2], Olivier Margeat[3], Jörg Ackermann[3] and Mats Fahlman[1]*

[1] Department of Physics, Chemistry and Biology, Linköping University, SE-58183 Linköping, Sweden

[2] Genes'Ink, 24 Av. Gaston Imbert, 13790 Rousset, France

[3] Aix-Marseille Université, CNRS, CINaM UMR 7325, 13288, Marseille, France.

Email: qinba@ifm.liu.se

Abstract:

We systematically show the effect of UV-light soaking on surface electronic structure and chemical states of solution processed ZnO nanoparticle (ZnONP) films in UHV, dry air and UV-ozone. UV exposure in UHV induces a slight decrease in work function and surface-desorption of chemisorbed oxygen, whereas UV exposure in presence of oxygen cause an increase in work function due to oxygen atom vacancy filling in the ZnO matrix. We demonstrate that UV-light soaking in combination with vacuum or oxygen can tune the work function of the ZnONP films over a range exceeding 1 eV. Based on photovoltaic performance and diode measurements, we conclude that the oxygen atom vacancy filling occurs mainly at the surface of the ZnONP films and that the films consequently retain their n-type behavior despite significant increase in measured work function.

Introduction

Polymer solar cell (PSC) is considered as a promising renewable energy technology because of properties such as light weight, flexibility, low cost at large production, and power conversion efficiency (PCE) close to 10% has been demonstrated.[1, 2] Conventional PSC geometry comprises an active layer based on nanosale donor/acceptor network sandwiched between a bottom indium tin oxide (ITO) modified by a hole conducting Poly(3,4-ethylenedioxythiophene): poly(styrenesulfonate) (PEDOT:PSS) as anode and a top low work function metal as cathode.[3] However, the strong acidic PEDOT:PSS etching and metal oxidation lead to a rapid degradation of PCE,[4-6] which obviously limits the operational lifetime of device. To address the drawbacks, significant advances have been focused on modification of device architecture and interlayer.[7, 8] The inverted device features a low work function interlayer *e.g.* a transition metal oxide (TiOx, ZnO),[9, 10] conjugated polymer (PFN, PFNBr),[11-13] or insulator (PEIE)[14] coated on ITO that acts as the bottom cathode and an air-stable high work function metal or metal oxide *e.g.* Au and MoOx as the top anode.[15, 16] In addition, the inverted structure also matches well with the vertical phase separation of the active bulk heterojunction layer and thus enhances charge collection at the organic/electrode interfaces.[17, 18]

Solution processed ZnO nanoparticle (ZnONP) layers are widely used as cathodes for the inverted polymer solar cells[19, 20] and n-type side of the recombination layer in tandem architectures[21, 22] due to comparatively high electron conductivity, low work function, transparency and environmental stability. The use of ZnO layers is not without problems, however. The conductivity of ZnO films is thought to be negatively affected by chemisorbed oxygen and this can in turn negatively impact the efficiency of the PCS.[23] The surface conductivity of ZnO films is decreased as chemisorbed oxygen molecules capture electrons from the ZnO conduction band creating a near-surface depletion region with a then

comparatively high resistivity.[24-26] Oxygen molecules can also diffuse into the ZnO film where they chemisorb and create a potential barrier between and a depletion region along either side of the grain boundary, thus reducing the bulk conductivity of the film.[24-26] Ultra violet (UV) light-soaking of a ZnO film can improve conductivity as the photo-generated holes in the ZnO can discharge the negatively charged chemisorbed oxygen molecules thereby desorbing them at both the surface and grain boundaries.[24-26] When the ZnO layer is formed from ZnO nanoparticle (NP) formulations, the effect of chemisorbed oxygen on conductivity can take on even larger importance as the porosity of such ZnO films makes oxygen diffusion and surface chemisorption even bigger issues. UV light-soaking is thus often used in PSC featuring ZnO electron transport layers in order to improve the conductivity of the ZnO layer and decrease the series resistance, as well as eliminate the formation of S-shape current-voltage characterization as a result of kinetic barriers to charge transport at the contact,[27] and hence enhance the efficiency of the device.[23] However, the excessive UV light-soaking would strongly modify the ZnONP work function, thus cause the interfacial band alignment shift in companying with the device performance degradation.[28-32]

Previous work has demonstrated that the photovoltaic performance is sensitive to the surface electronic structure of cathode interlayer in terms of aligning energy levels at the interface with the bulk heterojunction layer.[33] ZnONP provides well matching contact energetics with the active layer as the typical work function of ~ 4.0 eV[34, 35] is low enough to pin the Fermi level at the fullerene interface [36-39], facilitating photoinduced electron transfer and extraction from polymer:fullerene blend. The low-lying ZnONP valence band of ~ 7.6 eV[40, 41] relative to vacuum level can effectively prevent holes from the blend reaching cathode for recombination, further reducing loss in PSC efficiency.

In this work we use UV light soaking and UV-ozone treatment to tune the work function (WF) of ZnONP films and correlate the WF modification with the surface electronic structure and

chemical composition of the ZnONP. Three different soaking conditions are used (i) UV in ultrahigh vacuum (UHV), (ii) UV in dry air and (iii) UV-ozone. Moreover, we explore the effect of UV-ozone treatment on PSC performance in both conventional and inverted architecture devices.

Results and Discussion

Fig.1 shows the ultraviolet photoelectron spectroscopy (UPS) derived work functions ($\Phi_{ZnONP/sub}$) for a series of ZnONP films spin-coated onto the various substrates (Φ_{sub}) featuring work function from 3.9 to 5.6 eV. Clearly, the ZnONP film surface electronic structure is not dependent on the underlying substrate and the resulting work function keep constant 3.85 ± 0.05 eV. It also excludes ascribing any change in work function from UV/UV-ozone soaking of ZnONP film work function to potential energy change at the ZnONP/conducting substrate contact. When the ZnONP interlayer is inserted between the active layer and conducting substrates in a PSC, an Ohmic contact thus is formed at the fullerene/ZnONP interface [36-39], whereas the IP of 7.75 ± 0.05 eV is high enough to block hole extraction at the donor polymer/ZnONP interface.

Fig. 2a depicts the UPS spectra evolution of ZnONP film as a function of UV soaking time in UHV. The bottom spectrum corresponds to the pristine film. Its work function and the ionization potential (IP) are estimated to be 3.88 and 7.75 eV, respectively, within the range of previous reported values[42] and ~ average for the series of formulations studies (see Table S1). Upon exposure, an abrupt vacuum level downshift of ~ 0.1 eV is observed as the work function decreases from 3.88 to 3.77 eV, where it stabilizes after 180 min. Concurrently, the valence band undergoes an almost negligible downshift of only ~ 0.02 eV at saturation, leading to the overall IP decrease as shown in Fig. 2b and c. There is only a slight difference in the valence feature after UV soaking in the insert of Fig. 2a, which arises from hybridized

Zn*4s* and *4p*, and O*2p* contributions.[43] X-ray photoelectron spectroscopy (XPS) is further applied to exam the surface chemical states. The Zn$2p_{3/2}$ core level, located at binding energy of 1022.65 eV, is unaffected by the UV soaking (Fig. 1d). In the asymmetric O*1s* core level spectra the peak at lower binding energy of 531.36 eV represents O atoms in a ZnO matrix (Zn-O bonds), and the shoulder peak at higher binding energy of 532.93 eV is assigned to oxygen-defect sites related to oxygen atom vacancies in the matrix and chemisorbed oxygen attributed to the surrounding Zn atoms screening the O^{2-}*1s* photoelectron with lower kinetic energy compared to the main peak in a ZnO matrix.[44] After UV soaking in UHV, the oxygen-defect component decreases, as expected since the photogenerated holes in the ZnONP contribute to desorption of the oxygen molecules at the surfaces of the nanoparticles as mentioned in the introduction. Desorption of the previously negatively charged oxygen molecules from the surface also decreases the accompanying potential step, explaining the decrease in WF.

The UV-induced behavior in dry air as shown in Fig. 3a differs dramatically from the case of UHV. With increasing UV light soaking time, the work function of ZnONP gradually increases so that it reaches 4.29 eV after 180 min, and the valence band edge relative to the Fermi level conversely shifts towards lower energy from 3.9 to 3.58 eV (Fig. 3b), resulting in an overall increase in IP (Fig.3c). Both of Zn*2p3/2* and O*1s* core level spectra shift towards lower binding energy vs Fermi level by approximately 0.4 eV, and this shift mainly results from the work function variation (Fig. 3d and e). Additionally, a significant decrease in the intensity of the oxygen-defect feature and a slight increase in the intensity of the Zn-O feature were observed (Fig. 3e), the latter likely is due to ZnONP interacting with the small amount of ozone generated through the UV irritation in an O_2 containing medium. The similar and amplified phenomenon is obtained through UV-ozone soaking, see Fig.4, supporting this speculation. Fig.4a shows the UPS spectra obtained of ZnONP film as a function of UV-

ozone soaking time. The work function sharply increases up to 4.8 eV and the valence band decreases to 3.49 eV within 120 min, leading to an overall upshift of the IP (Fig. 4b and c). It should be stressed that there is no saturation trend in work function and IP, but the valence band edge energy stays constant after 10 min soaking. A new feature centered at 8.0 eV in valence band region appears due to the increase of O*2p* state intensity,[43] which implies filling of oxygen vacancies by oxygen introduced by UV-ozone. Considering that the lack of oxygen stoichiometry makes ZnONP as n-type semiconductor due to the oxygen defects,[45] the surface of ZnONP becomes less conducting during UV-ozone soaking [24, 25] and less n-type, in agreement with the observed increase in WF and the smaller energy offset between valence band and Fermi level in the case of the constant band gap. No obvious changes were observed in the Zn*2p* core level spectra except for a shift of 0.6 eV to lower binding energy (Fig.4d). This shift results from the combination of more Zn atoms bound to O atoms and the WF shift. Because of the oxygen vacancy filling under UV-ozone, the intensity of the oxygen-deficient sites and the intensity corresponding to the Zn-O bonds show the significant decrease and increase, respectively (Fig.4e). These results imply that UV-light soaking in presence of O_2/ozone significantly modifies the surface chemical composition and the surface electronic properties in comparison with UV light soaking in UHV of ZnONP films, since the desorption of oxygen molecules is accompanied with filling of oxygen atom vacancies in the ZnO matrix.

To explore the influence of surface chemical and electronic properties of ZnONP layers on photovoltaic performance, current density-voltage (J-V) characteristics of both conventional and inverted solar cells incorporating ZnONP layer as anode and cathode interlayers respectively under AM 1.5 G irradiation with intensity of 100mW/cm^2 and in dark are shown in Fig.5 and 6. The ZnONP layers used were either pristine or UV-ozone treated. Table 1 summarizes the performance parameters.

In the inverted solar cell, the J-V characteristics of ITO/ZnONP (pristine and UV-ozone soaking)/TQ1:$PC_{70}BM$/MoO_3/Al devices are shown in Fig. 5a. After ZnONP UV-ozone soaking, the open voltage (V_{oc}) decreased from 0.82 to 0.65 eV, the fill factor (FF) from 53.8% to 48.8% and PCE from 3.76% to 2.83%. Noticeably, the current density (J_{sc}) increased from 8.41 to 8.99 mA/cm^2. The trends of these parameters are similar with the recent report by J. M. Cho et al.[30] The decreased FF could be accounted for by analyzing the dark J-V curves in Fig. 5b. An augmented dark current is observed in the device using the UV-ozone exposed ZnONP. To investigate this origin of the V_{oc} and J_{sc} change, we picture the energy level alignments at ZnONP/$PC_{70}BM$ interface before and after UV-ozone soaking (Fig. 5c and d). The work function of the pristine ZnONP (3.88 eV) is smaller than the energy of negative ICT state of $PC_{70}BM$ (E_{ICT-} = 4.35 eV),[46] the Fermi level pins to the ICT^- state causing a potential step that upshifts the vacuum level, forming an Ohmic contact at $PC_{70}BM$/ZnONP interface. Upon UV-ozone exposure, the vacuum level (VL) alignment holds following Schottky-Mott rule due to $\Phi_{ZnONP} > E_{ICT-}$ of $PC_{70}BM$. The observed V_{oc} loss could be ascribed to the increase of work function on ZnONP surface, which on the one hand breaks Ohmic contact at $PC_{70}BM$/ZnONP interface causing an electron-extraction barrier, resulting in a smaller built-in potential. However, it cannot be a factor for the J_{sc} enhancement. Previous reports have ruled out that the morphology of the subsequent active layer effect after ZnONP UV-ozone soaking,[35] and the ZnO-ozone interaction counteract the conductivity improvement from the UV exposure.[24, 25] The UV-ozone exposure not only increases the work function, but also passivates the surface defects of ZnONP by ozone-interaction-induced filling of oxygen vacancies (Fig. 4e). This modification would reduce the carrier recombination at the ZnONP/active layer interface, resulting in an increase both in carrier lifetime and photocurrent.[47]

The high WF of UV-ozone soaked ZnONP films is attributed mainly to the filling of oxygen atom vacancies, reducing the number of electrons in the conduction band and thus pushing the Fermi level more towards the center of the band gap. It is thus a tempting thought that this process could be used to convert the ZnO into more of a p-type semiconductor which then would be suitable as a transparent anode. The p-type performance cannot be concluded from just a marked shift in the Fermi energy towards the valence band, however, so we tested the concept in a conventional geometry where the ZnONP layer replaces the PEDOT:PSS. For the reference PCE device with ITO/PEDOT:PSS/TQ1:$PC_{70}BM$/LiF/Al as the multilayer stack, a V_{oc} of 0.89 V, Jsc of 9.0 mA/cm^2 and FF of 68.8% are easily achieved, giving a typical PCE of 5.51%. As a comparison, when using instead an UV-ozone exposed ZnONP layer with high work function of 4.8 eV, the device performance significantly drops, producing V_{oc}, J_{sc}, FF and PCE that are only 0.13 V, 5.5 mA/cm^2, 40.5% and 0.29%, respectively (Fig. 6a). The dark current increases by two orders of magnitude in spite of the high work function of UV-ozone ZnONP. Note that the work function of PEDOT:PSS (~ 5.1 eV) and the UV-ozone ZnONP (~ 4.8 eV) are larger than the energy of positive integer charge states (E_{ICT+}) of donor TQ1 (~ 4.3 eV).[46] Hence, as per ICT model,[48] a potential step is created at interface by spontaneous charge transfer via tunneling across interface from donor to anode pinning the Fermi level to the ICT^+ state of the donor for both PEDOT:PSS and UV-ozone ZnONP. The valence band edge of UV-ozone ZnONP, though now closer to the Fermi level, still pose a significant barrier towards hole extraction (see Fig.S3), however. Furthermore, though the UV-ozone soaking induced oxygen vacancy filling substantially reduces the defect density at the surface of the ZnONP, the bulk vacancy density if largely unaffected, would still make the ZnONP films n-type and hence unsuitable as anode material. The surface sensitivity of the photoelectron spectroscopy techniques used prevent effective probing of the bulk properties of the films, so to explore this point we instead carried out charge transport measurement

using diode structures of ITO/PEDOT:PSS and UV-ozone exposed ZnONP/MEH-PPV/Au (see Fig. S2), confirming n-type behavior of the ZnONP films even after UV-ozone soaking, suggesting the effects are mainly concentrated to the surface.

Conclusion:

We have systematically investigated the effect of UV-light soaking on surface electronic structures and chemical states of solution processed ZnONP film in UHV, dry air and UV-ozone. We find that its surface properties are very sensitive to the UV irradiation. UV soaking in UHV induces a slight decrease in both work function and oxygen-deficient component, and an almost negligible downshift in valence band. For UV-light soaking in presence of oxygen, the work function increases accompanied by a smaller energy offset between the valence band edge and Fermi level. A decrease of the oxygen-defect component and a slight increase of the ZnO matrix feature are observed, attributed to desorption of oxygen molecules from the surface and filling of oxygen atoms in the ZnO matrix. The work function of ZnONP films can be tuned over a range spanning more than 1 eV using this technique. We also reported the effect of the strong surface modification of the UV-ozone exposed ZnONP on photovoltaic performance and concluded that the high work function ZnONP films retain their n-type behavior as the oxygen vacancy filling from the UV-ozone soaking seems concentrated to the surface of the films. Enhancement in J_{sc} can be obtained by UV-soaking of ZnONP cathode layers as filling of surface vacancies reduce carrier recombination at the fullerene/ZnONP interface.

Experimental details

Photoelectron spectroscopy: ZnO nanoparticle solutions in the study were prepared by Genes'Ink (particle size < 10 nm) and prepared by CNRS (particle size ~6 nm). The CNRS

ZnONP solutions are based on ZnO nanoparticles synthesized by a modified procedure[49] using ethanolamine as surface ligand in isopropanol[50]. Thin films (~15 nm) were spin-coated onto different conducting substrates from the solutions. The UV-light soaking photoelectron spectroscopy experiments used a Genes'Ink ZnONP solution spincoated onto indium tin oxide substrate. For UV-light soaking in UHV, sample was placed in a preparation chamber with a base pressure of 8×10^{-10} mbar and 365 nm UV irradiation emitted from a 12 W lamp transmitted through the UV Zero viewport (Ultimate vacuum), then sample was directly transferred to analysis chamber for photoelectron spectroscopy measurement without breaking vacuum. The UV-ozone treatment was made in a UVO-cleaner (Model No. 42-220) from Jelight Company, Inc. UPS (HeI *hv* = 21.22 eV) and XPS (monochromatized Al Ka *hv* = 1486.6 eV) spectra were recorded with a Scienta-200 hemispherical analyzer and calibrated by determining Fermi level edge of the Ar^+ ion sputter-cleaned Au foil. UPS was performed to characterize work function and the frontier electronic features, and the spectra were quickly collected to shield of the intrinsic UV source. The work function is derived from the secondary electron cut-off and the vertical ionization potential (IP) from the frontier edge of the occupied density of states. XPS was used to detect the surface chemical states before and after soaking.

Device fabrication and characterization: TQ1 was synthesized at Chalmers University of Technology, and $PC_{70}BM$ was purchased from Solenne BV. The structure for the normal device configuration is ITO/PEODT:PSS (or UV-ozone exposed ZnONP)/active layer/LiF /Al, and that for the inverted device configuration is ITO/ZnO (or UV-ozone exposed ZnONP)/active layer/MoO_3/Al. The interlayer PEDOT:PSS (Heraeus, Clevios P VP Al 4083) was annealed at 120 °C for 20 min after spin-coating, and the interlayer ZnONP was annealed at 110 °C for 10 min after spin-coating. The active layer (a blend of TQ1 and $PC_{70}BM$ with a weight ratio of 1:2.5) was spin-coated from the 1,2-dichlorobenzene solution (total

concentration of 35mg/ml) with a final film thickness of ~ 80 nm. The structure for the diode is ITO/interlayer/MEH-PPV/Au (80nm), where the interlayer is either PEDOT:PSS or UV-ozone exposed ZnONP. MEH-PPV (Sigma-Aldrich) was spin-coated from the 1,2-dichlorobenzene solution (concentration of 10 mg/ml) with a final film thickness of ~100 nm. The current density–voltage (J –V) characteristics of the devices were measured using a Keithley 2400 source meter with a simulated AM1.5 solar illumination (100 mW cm^{-2}). The solar simulator was calibrated with a reference Si cell (SRC-1000-RTD) prior to the measurements.

Acknowledgments: We acknowledge the support from the EU project SUNFLOWER of FP7 cooperation programme, grant agreement number 287594. X.L. acknowledges support from The Swedish Research Council Linnaeus grant LiLi-NFM.

Reference

1. Z. C. He, C. M. Zhong, S. J. Su, M. Xu, H. B. Wu and Y. Cao, *Nat. Photonics*, 2012, **6**, 591-595.
2. J. B. You, L. T. Dou, K. Yoshimura, T. Kato, K. Ohya, T. Moriarty, K. Emery, C. C. Chen, J. Gao, G. Li and Y. Yang, *Nat. Commun.*, 2013, **4**, 1446.
3. G. Yu, J. Gao, J. C. Hummelen, F. Wudl and A. J. Heeger, *Science*, 1995, **270**, 1789-1791.
4. M. P. de Jong, L. J. van IJzendoorn and M. J. A. de Voigt, *Appl. Phys. Lett.*, 2000, **77**, 2255-2257.
5. M. Jorgensen, K. Norrman and F. C. Krebs, *Sol. Energ. Mat. Sol. C.*, 2008, **92**, 686-714.
6. K. Kawano, R. Pacios, D. Poplavskyy, J. Nelson, D. D. C. Bradley and J. R. Durrant, *SoL. Energ. Mat. Sol. C.*, 2006, **90**, 3520-3530.
7. S. K. Hau, H. L. Yip and A. K. Y. Jen, *Polym. Rev.*, 2010, **50**, 474-510.
8. C. H. Hsieh, Y. J. Cheng, P. J. Li, C. H. Chen, M. Dubosc, R. M. Liang and C. S. Hsu, *J. Am. Chem. Soc.*, 2010, **132**, 4887-4893.
9. Y. M. Sun, J. H. Seo, C. J. Takacs, J. Seifter and A. J. Heeger, *Adv. Mater.*, 2011, **23**, 1679.
10. C. Waldauf, M. Morana, P. Denk, P. Schilinsky, K. Coakley, S. A. Choulis and C. J. Brabec, *App. Phys. Lett.*, 2006, **89**, 233517.
11. T. B. Yang, M. Wang, C. H. Duan, X. W. Hu, L. Huang, J. B. Peng, F. Huang and X. Gong, *Energ. Environ. Sci.* , 2012, **5**, 8208-8214.
12. Z. Tang, L. M. Andersson, Z. George, K. Vandewal, K. Tvingstedt, P. Heriksson, R. Kroon, M. R. Andersson and O. Inganas, *Adv. Mater.*, 2012, **24**, 554.

13. R. D. Xia, D. S. Leem, T. Kirchartz, S. Spencer, C. Murphy, Z. C. He, H. B. Wu, S. J. Su, Y. Cao, J. S. Kim, J. C. deMello, D. D. C. Bradley and J. Nelson, *Adv. Enery. Mater.*, 2013, **3**, 718-723.
14. Y. H. Zhou, C. Fuentes-Hernandez, J. Shim, J. Meyer, A. J. Giordano, H. Li, P. Winget, T. Papadopoulos, H. Cheun, J. Kim, M. Fenoll, A. Dindar, W. Haske, E. Najafabadi, T. M. Khan, H. Sojoudi, S. Barlow, S. Graham, J. L. Bredas, S. R. Marder, A. Kahn and B. Kippelen, *Science*, 2012, **336**, 327-332.
15. C. Tao, S. P. Ruan, X. D. Zhang, G. H. Xie, L. Shen, X. Z. Kong, W. Dong, C. X. Liu and W. Y. Chen, *Appl. Phys. Lett.*, 2008, **93**, 193307.
16. J. Kim, D. Y. Khang, J. H. Kim and H. H. Lee, *Appl. Phys. Lett.*, 2008, **92**, 133307.
17. Z. Xu, L. M. Chen, G. W. Yang, C. H. Huang, J. H. Hou, Y. Wu, G. Li, C. S. Hsu and Y. Yang, *Adv Funct Mater*, 2009, **19**, 1227-1234.
18. M. Campoy-Quiles, T. Ferenczi, T. Agostinelli, P. G. Etchegoin, Y. Kim, T. D. Anthopoulos, P. N. Stavrinou, D. D. C. Bradley and J. Nelson, *Nat. Mater.*, 2008, **7**, 158-164.
19. M. S. White, D. C. Olson, S. E. Shaheen, N. Kopidakis and D. S. Ginley, *Appl. Phys. Lett.*, 2006, **89**, 143517.
20. T. B. Yang, W. Z. Cai, D. H. Qin, E. G. Wang, L. F. Lan, X. Gong, J. B. Peng and Y. Cao, *J. Phys. Chem. C*, 2010, **114**, 6849-6853.
21. V. S. Gevaerts, A. Furlan, M. M. Wienk, M. Turbiez and R. A. J. Janssen, *Adv. Mater.*, 2012, **24**, 2130-2134.
22. S. Kouijzer, S. Esiner, C. H. Frijters, M. Turbiez, M. M. Wienk and R. A. J. Janssen, *Adv. Energy. Mater.*, 2012, **2**, 945-949.
23. H. Cheun, C. Fuentes-Hernandez, Y. H. Zhou, W. J. Potscavage, S. J. Kim, J. Shim, A. Dindar and B. Kippelen, *J. Phys. Chem. C*, 2010, **114**, 20713-20718.
24. G. Goncalves, A. Pimentel, E. Fortunato, R. Martins, E. L. Queiroz, R. F. Bianchi and R. M. Faria, *J. Non-Cryst. Solids*, 2006, **352**, 1444-1447.
25. R. Martins, E. Fortunato, P. Nunes, I. Ferreira, A. Marques, M. Bender, N. Katsarakis, V. Cimalla and G. Kiriakidis, *J. Appl. Phys.*, 2004, **96**, 1398-1408.
26. I. V. Tudose, P. Horvath, M. Suchea, S. Christoulakis, T. Kitsopoulos and G. Kiriakidis, *Appl. Phys. A-Mater. Sci. Process.*, 2007, **89**, 57-61.
27. S. R. Cowan, P. Schulz, A. J. Giordano, A. Garcia, B. A. MacLeod, S. R. Marder, A. Kahn, D. S. Ginley, E. L. Ratcliff and D. C. Olson, *Adv Funct Mater*, 2014, **24**, 4671-4680.
28. D. C. Olson, Y. J. Lee, M. S. White, N. Kopidakis, S. E. Shaheen, D. S. Ginley, J. A. Voigt and J. W. P. Hsu, *J Phys Chem C*, 2008, **112**, 9544-9547.
29. J. J. Uhlrich, D. C. Olson, J. W. P. Hsu and T. F. Kuech, *J Vac Sci Technol A*, 2009, **27**, 328-335.
30. J. M. Cho, S.-W. Kwak, H. Aqoma, J. W. Kim, W. S. Shin, S.-J. Moon, S.-Y. Jang and J. Jo, *Org. Electron.*, 2014, **15**, 1942-1950.
31. A. Manor, E. A. Katz, T. Tromholt and F. C. Krebs, *Adv. Energy Mater.*, 2011, **1**, 836-843.
32. A. Manor, E. A. Katz, T. Tromholt and F. C. Krebs, *Sol. Energy Mat. Sol. C.*, 2012, **98**, 491-493.
33. H. Ma, H. L. Yip, F. Huang and A. K. Y. Jen, *Adv Funct Mater*, 2010, **20**, 1371-1388.
34. J. Hu, Z. W. Wu, H. X. Wei, T. Song and B. Q. Sun, *Org. Electron.*, 2012, **13**, 1171-1177.
35. S. Bai, Z. W. Wu, X. L. Xu, Y. Z. Jin, B. Q. Sun, X. J. Guo, S. S. He, X. Wang, Z. Z. Ye, H. X. Wei, X. Y. Han and W. L. Ma, *Appl. Phys. Lett.*, 2012, **100**.
36. H. Aarnio, P. Sehati, S. Braun, M. Nyman, M. P. de Jong, M. Fahlman and R. Osterbacka, *Adv. Energy. Mater.*, 2011, **1**, 792-797.
37. L. M. Chen, Z. R. Hong, G. Li and Y. Yang, *Adv. Mater.*, 2009, **21**, 1434-1449.
38. R. J. Davis, M. T. Lloyd, S. R. Ferreira, M. J. Bruzek, S. E. Watkins, L. Lindell, P. Sehati, M. Fahlman, J. E. Anthony and J. W. P. Hsu, *J. Mater. Chem.*, 2011, **21**, 1721-1729.
39. M. Fahlman, P. Sehati, W. Osikowicz, S. Braun, M. P. de Jong and G. Brocks, *J. Electron Spectrosc. Relat. Phenom.*, 2013, **190**, 33-41.
40. P. P. Boix, J. Ajuria, I. Etxebarria, R. Pacios, G. Garcia-Belmonte and J. Bisquert, *J. Phys. Chem. Lett.*, 2011, **2**, 407-411.
41. H. L. Yip, S. K. Hau, N. S. Baek, H. Ma and A. K. Y. Jen, *Adv. Mater.*, 2008, **20**, 2376.

42. M. J. Tan, S. Zhong, J. Li, Z. K. Chen and W. Chen, *Acs Appl. Mater. Inter.*, 2013, **5**, 4696-4701.
43. W. M. Tang, M. T. Greiner, Z. H. Lu, W. T. Ng and H. G. Nam, *Thin Solid Films*, 2011, **520**, 569-573.
44. J. C. C. Fan and J. B. Goodenough, *J. Appl. Phys.*, 1977, **48**, 3524.
45. D. L. Raimondi and E. Kay, *J. Vac. Sci. Technol.*, 1969, **7**, 96.
46. Q. Y. Bao, O. Sandberg, D. Dagnelund, S. Sanden, S. Braun, H. Aarnio, X. J. Liu, W. M. Chen, R. Österbacka and M. Fahlman, *Adv Funct Mater*, 2014, DOI: 10.1002/adfm.201401513
47. S. Chen, C. E. Small, C. M. Amb, J. Subbiah, T. H. Lai, S. W. Tsang, J. R. Manders, J. R. Reynolds and F. So, *Adv. Energ. Mater.*, 2012, **2**, 1333-1337.
48. S. Braun, W. R. Salaneck and M. Fahlman, *Adv. Mater.*, 2009, **21**, 1450-1472.
49. A. K. Diallo, M. Gaceur, N. Berton, O. Margeat, J. Ackermann and C. Videlot-Ackermann, *Superlattices and Microstructures*, 2013, **58**, 144-153.
50. G. Mattioli, S. B. Dkhil, M. I. Saba, G. Malloci, C. Melis, P. Alippi, F. Filippone, P. Giannozzi, A. K. Thakur, M. Gaceur, O. Margeat, A. K. Diallo, C. Videlot-Ackermann, J. Ackermann, A. A. Bonapasta and A. Mattoni, *Adv. Energy Mater.*, 2014, DOI: 10.1002/aenm.201301694.

Figure

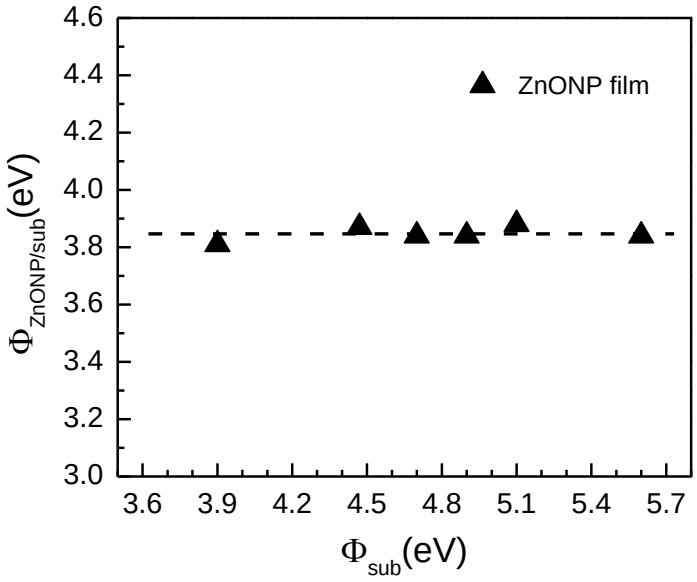

Fig.1 Work function for a series of ZnONP films spin-coated onto the various substrates featuring work function from 3.9 to 5.6 eV.

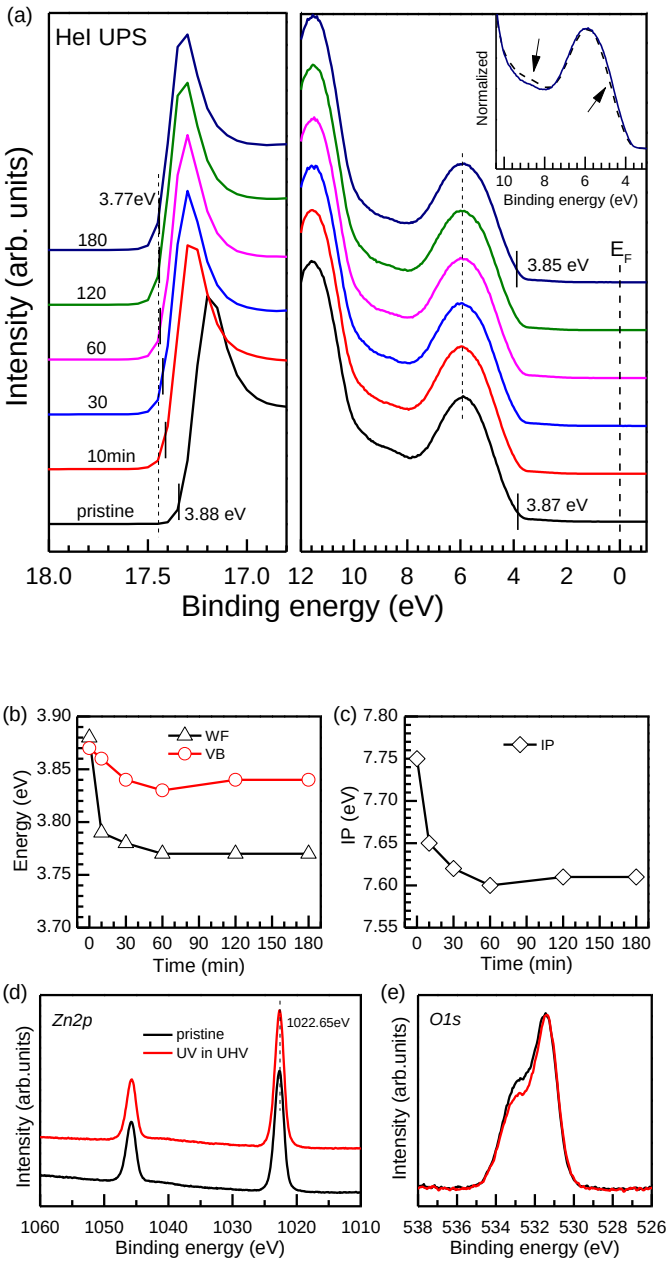

Fig. 2. (a) UPS spectra evolution at the secondary electron region and the frontier electronic structure region of ZnONP film as a function of UV-light soaking time in UHV; (b) summary of the work function and valence band edge energies and (c) IP dependence on soaking time; (d) and (e) XPS Zn*2p* and O*1s* core level spectra before and after 180 min UV soaking in UHV. The inset indicates the slight difference in the valence feature after UV soaking.

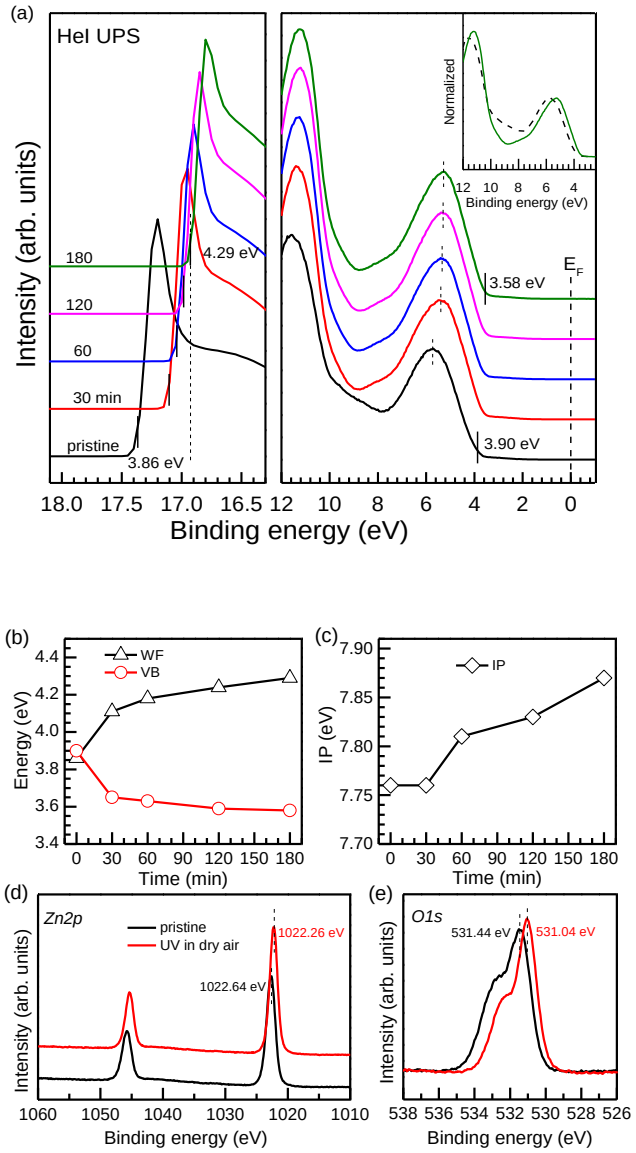

Fig. 3 (a) UPS spectra evolution at the secondary electron region and the frontier electronic structure region of ZnONP film as a function of UV-light soaking time in dry air; (b) summary of the work function and valance band edge energies and (c) IP dependence on soaking time; (d) and (e) XPS Zn*2p* and O*1s* core level spectra before and after 180 min UV soaking in dry air. The insert indicates the clear difference in the valence feature after UV soaking.

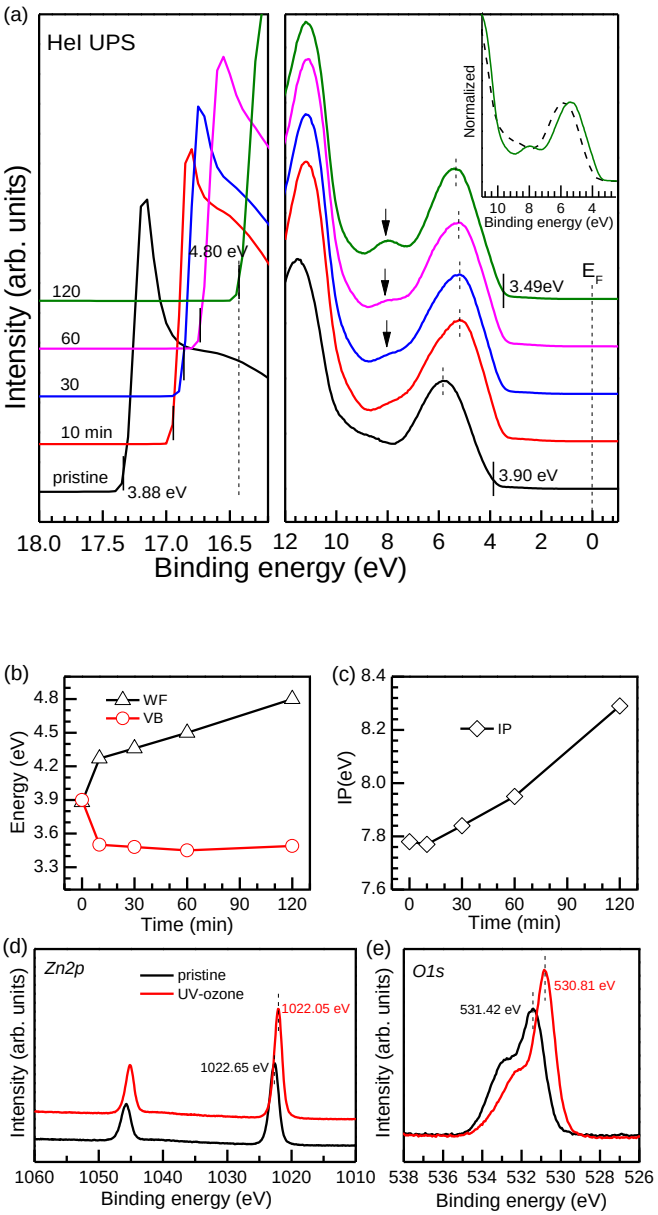

Fig. 4 (a) UPS spectra evolution at the secondary electron region and the frontier electronic structure region of ZnONP film as a function of UV-ozone soaking time; (b) summary of the work function and valance band edge energies and (c) IP dependence on soaking time; (d) and (e) XPS Zn*2p* and O*1s* core level spectra before and after 120 min UV-ozone soaking.

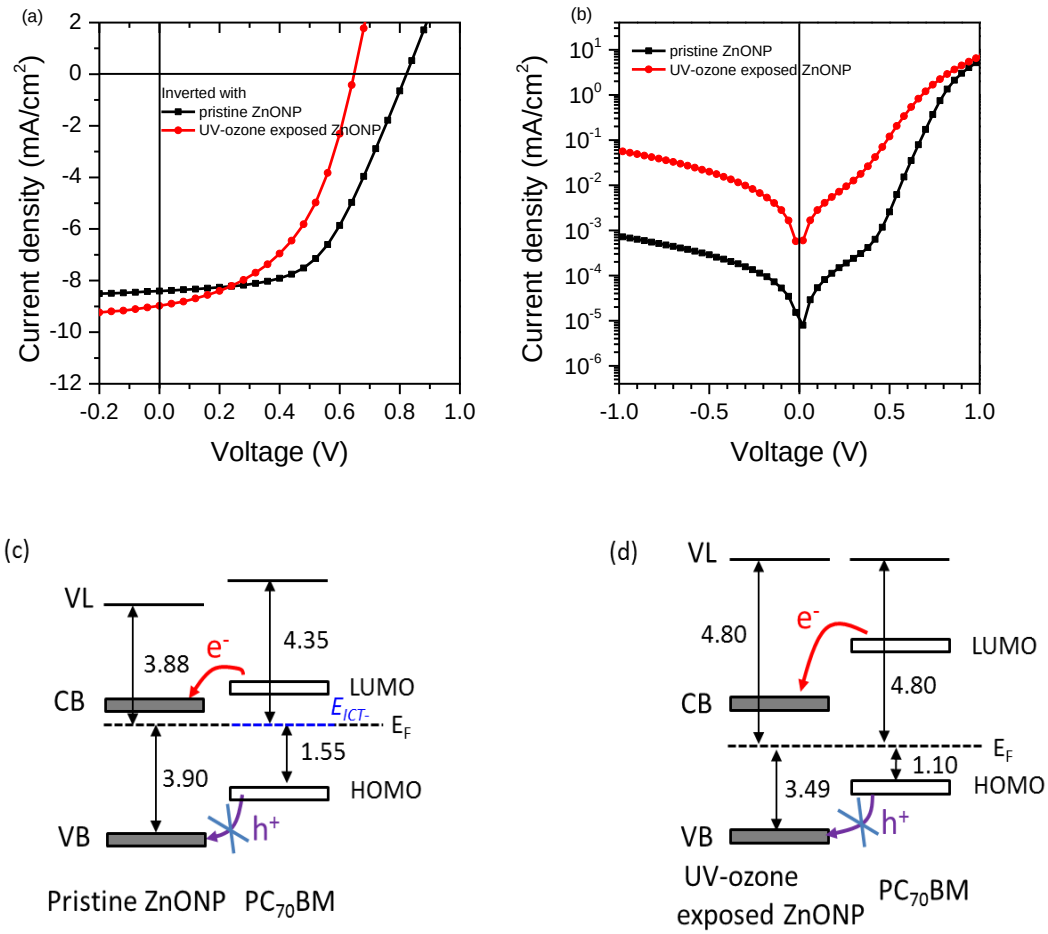

Fig. 5 (a) J-V characteristics of two inverted TQ1:$PC_{70}BM$ solar cells incorporating the pristine and UV-ozone exposed ZnONP as cathode; (b) Dark current of the inverted TQ1:$PC_{70}BM$ solar cells; (c) and (d) energy level alignment diagrams at $PC_{70}BM$/ZnONP (pristine and UV-ozone soaking) interfaces. Here, the ZnONP interlayer applied in device was UV-ozone soaked for 120 min.

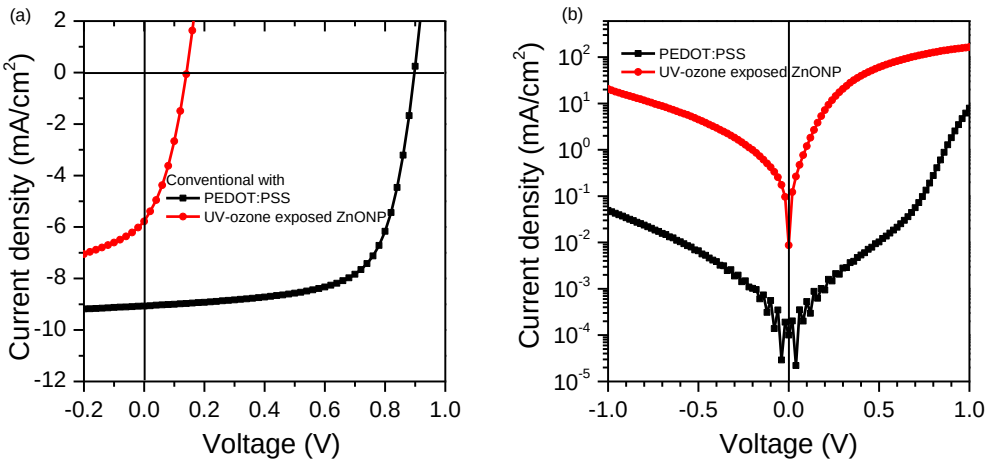

Fig. 6 (a) J-V characteristics of two conventional TQ1:$PC_{70}BM$ solar cells incorporating PEDOT:PSS and UV-ozone exposed ZnONP as anode; (b) Dark current of the conventional TQ1:$PC_{70}BM$ solar cells. Here, the ZnONP interlayer applied in device was UV-ozone soaked for 120 min.

Table 1: Photovoltaic performance of TQ1:$PC_{70}BM$ solar cells and their corresponding reference devices. The polymer TQ1 used in the conventional and inverted devices are respectively from the two batches.

	Voc (V)	*Jsc* (mA/cm^2)	FF (%)	PCE
Conventional with PEDOT:PSS	0.89	9.0	68.8	5.51
Conventional with UV-ozone exposed ZnONP	0.13	5.5	40.5	0.29
Inverted with pristine ZnONP	0.82	8.41	53.8	3.76
Inverted with UV-ozone exposed ZnONP	0.65	8.99	48.8	2.83

Table of contents entry: Effects of ultraviolet soaking on surface electronic structures of solution processed ZnO nanoparticle film in combination with vacuum or oxygen in polymer solar cell were researched.

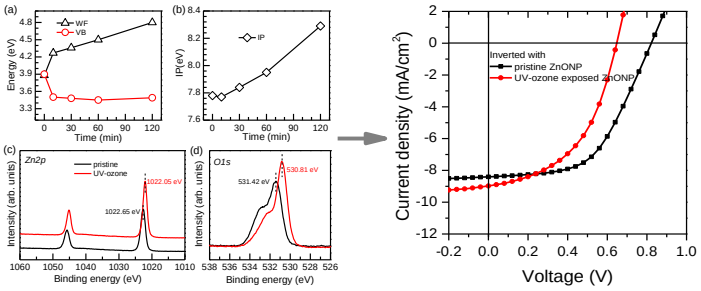

Supplementary information

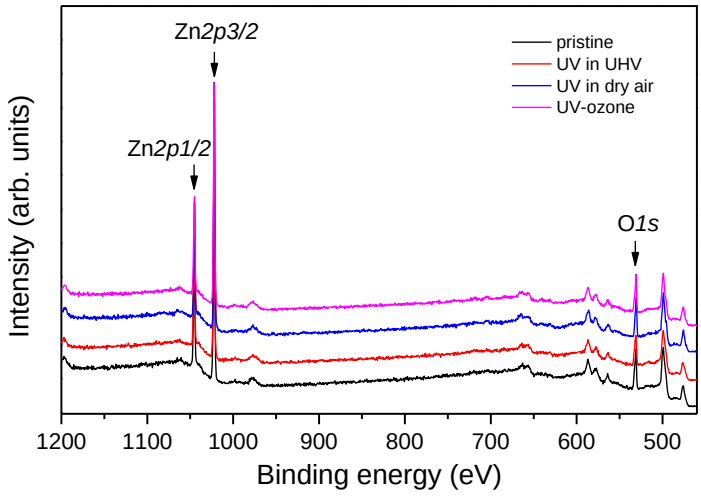

Fig. S1 XPS survey spectra of ZnONP film before and after UV-light soaking in UHV, dry air and UV-ozone.

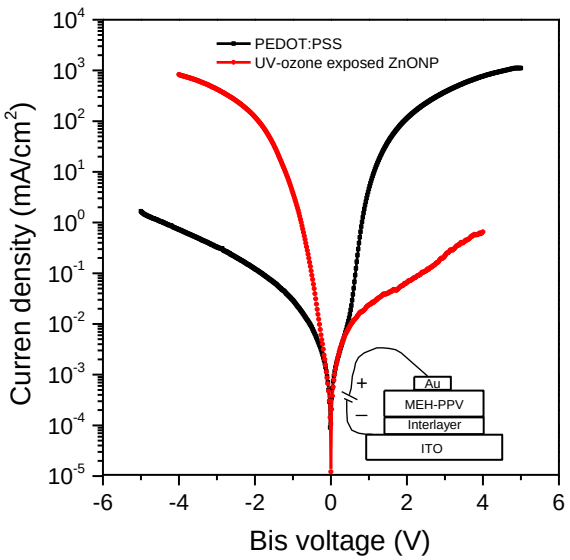

Fig. S2 J-V characteristics of the diode with structure of ITO/PEDOT:PSS or UV-ozone exposed ZnONP/MEH-PPV/Au .

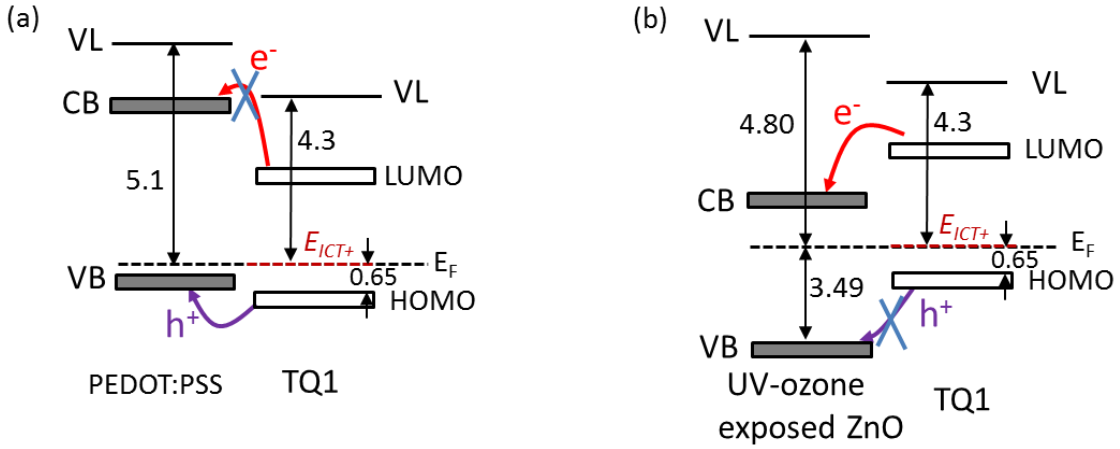

Fig. S3 Energy level alignment diagrams at (a) TQ1/PEDOT:PSS interface and (b) TQ1/UV-ozone exposed ZnONP interface.

Table S1: Work function (WF) and Ionization Potential (IP) measured by UPS for a series of ZnONP films spun-coated from solution, each row corresponding to a different ZnONP formulation, illustrating the range of WF and IP that can be obtained. The WF and IP values are obtained with an accuracy of ± 0.05 eV.

Supplier	**WF (eV)**	**IP (eV)**
Genes'Ink	3.88	7.84
Genes'Ink	4.00	7.83
Genes'Ink	3.97	7.88
Genes'Ink	3.90	7.89
Genes'Ink	3.96	7.92
Genes'Ink	3.60	7.94
Genes'Ink	3.65	7.77
Genes'Ink	3.81	7.74
Genes'Ink	3.67	7.63
Genes'Ink	3.93	7.95
Genes'Ink	3.79	7.82
Genes'Ink	3.75	7.83
CNRS	3.92	8.00
CNRS	3.98	8.03
CNRS	3.98	8.02
CNRS	3.89	7.98
CNRS	3.88	7.96
CNRS	4.02	7.66
CNRS	4.00	7.91